Journal of Controlled Release 362 (2023) 606–619

Contents lists available at ScienceDirect

Journal of Controlled Release

journal homepage: www.elsevier.com/locate/jconrel

Gene-activated hyaluronic acid-based cryogels for cartilage tissue engineering

Natalia Carballo-Pedrares [a], Junquera López-Seijas [a,b], Diego Miranda-Balbuena [a], Ibán Lamas [b], Julián Yáñez [b], Ana Rey-Rico [a,b,*]

[a] Gene & Cell Therapy Unit (G-CEL), Centro Interdisciplinar de Química e Bioloxía – CICA, Universidade da Coruña, As Carballeiras, s/n. Campus de Elviña, 15071 A Coruña, Spain

[b] Department of Biology, Facultade de Ciencias, Universidade da Coruña, Coruña, Spain

ARTICLE INFO

Keywords:
Cartilage repair
Gene therapy
Non-viral vectors
Niosomes
P80PX
Gene activated cryogel
HACG
Mesenchymal stem cells

ABSTRACT

Articular cartilage injuries are very frequent lesions that if left untreated may degenerate into osteoarthritis. Gene transfer to mesenchymal stem cells (MSCs) provides a powerful approach to treat these lesions by promoting their chondrogenic differentiation into the appropriate cartilage phenotype. Non-viral vectors constitute the safest gene transfer tools, as they avoid important concerns of viral systems including immunogenicity and insertional mutagenesis. However, non-viral gene transfer usually led to lower transfection efficiencies when compared with their viral counterparts. Biomaterial-guided gene delivery has emerged as a promising alternative to increase non-viral gene transfer efficiency by achieving sustained delivery of the candidate gene into cellular microenvironment. In the present study, we designed hyaluronic acid-based gene-activated cryogels (HACGs) encapsulating a novel formulation of non-viral vectors based on niosomes (P80PX) to promote MSCs *in situ* transfection. The developed HACG P80PX systems showed suitable physicochemical properties to promote MSCs *in situ* transfection with very low cytotoxicity. Incorporation of a plasmid encoding for the transcription factor SOX9 (p*sox9*) into HACG P80PX systems led to an effective MSCs chondrogenic differentiation with reduced expression of fibrocartilage and hypertrophic markers. The capacity of the developed systems to restore cartilage extracellular matrix was further confirmed in an *ex vivo* model of chondral defect.

1. Introduction

Traumatic joint diseases, which include mainly osteoarthritis (OA) and cartilage injuries, represent the primary cause of chronic disability in the USA, affecting >67 million people by 2030 [1]. In addition, the avascular and aneural nature of cartilage tissue strongly limits its ability to self-repair after injury [2]. Despite current therapeutical options to treat these disorders have notably been improved during last decades, none of these options have allowed restoring the natural functions of native hyaline cartilage [2]. Therefore, the design of new and effective approaches to treat cartilage lesions is under active investigation.

Gene therapy has emerged as a powerful approach to treat cartilage disorders by directly transferring genes encoding for therapeutic factors into the places of injury, that result in a temporarily and spatially defined delivery of the candidate gene [3]. Diverse non-viral and viral genetic vehicles have been tested to modify key cell populations involved in cartilage regenerative processes, such as chondrocytes and mesenchymal stem cells (MSCs) [2]. While non-viral vectors are considered the safest tools of gene transfer, avoiding important concerns of viral vehicles including the possibility to produce insertional mutagenesis or to trigger an immune response, their efficiency is still reduced when compared with their viral counterparts. Herein, the existence of extracellular and intracellular barriers such as serum neutralization, DNA internalization mechanism and trafficking or DNA *cargo* degradation by nucleases, strongly influence the obtaining of an effective transfection [4].

The design of non-viral gene delivery systems constitutes a promising tool to overcome these issues by maintaining elevated concentrations of vectors into the cellular environment, while protecting them against degradation [3]. Particularly, the use of gene-activated matrices (GAMs) emerged in 1996 [5] as a way to achieve direct, local, and sustained delivery of nucleic acids from a scaffold to ensure efficient and durable

* Corresponding author at: Gene & Cell Therapy Unit (G-CEL), Centro Interdisciplinar de Química e Bioloxía – CICA, Universidade da Coruña, As Carballeiras, s/n. Campus de Elviña, 15071 A Coruña, Spain.
E-mail address: ana.rey.rico@udc.es (A. Rey-Rico).

https://doi.org/10.1016/j.jconrel.2023.09.008
Received 13 March 2023; Received in revised form 28 July 2023; Accepted 3 September 2023
Available online 11 September 2023

cell transfection [6]. In this scenario, both chondral and osteochondral units are especially attractive for biomaterial-guided gene delivery approaches because of the limited blood flow to the region, which can cause problems in DNA complex delivery [7,8].

Gene delivery in GAMs involved the loading of the gene of interest with a carrier to avoid its degradation by extracellular nucleases or intracellular lysosomes in order to achieve an effective transfection of the target cell population [4]. Niosomes have been shown to be promising carriers to this end due to their higher stability and lower cytotoxicity when compared with classical liposomes. These properties have been attributed to their different chemical composition by substituting the phospholipids of liposomes for non-ionic surfactants in niosomes. Thereby, recent studies developed in our group demonstrated the potential of niosomes to successfully transfect human MSCs [9] and induce an effective chondrogenesis [10].

As an integral component of the GAM system, the scaffold material structure is essential to allow cell survival, adhesion, infiltration, and proliferation. Specifically, cryogels constitute a class of biomaterials with potential features over conventional hydrogels due to their macroporous structure and highly hydrated core, mimicking extracellular matrix cartilage composition [11]. Cryogels are normally produced by gelation at subzero temperatures, a process known as cryogelation, leading to the formation of macroporous structures with appropriate mechanical properties and shape memory ability [12]. Hereof, the interconnected macroporous structure in cryogels seems to facilitate cell infiltration and trafficking [12]. Remarkably, hyaluronic acid (HA) has been shown to be a potential biopolymer for cryogel fabrication in cartilage reparative approaches, due to its biodegradability, biocompatibility and non immunogenicity, being a ubiquitous compound of the cartilage extracellular matrix [13]. Moreover, HA has proved to interact with stem cell receptors modulating cell proliferation, survival, and differentiation [13].

Hence, in the present study, we designed, for the first time to the best of our knowledge, gene-activated cryogels (G-HACG) based on the combination of P80PX nioplexes with HA cryogels (G-HACG P80PX) to promote *in situ* transfection of MSCs. Therefore, once selected the optimal formulation ratio to transfect MSCs, P80PX nioplexes, and cells were incorporated into cryogels by freeze-drying in two steps. The developed G-HACG P80PX systems were physicochemically characterized exhibiting ideal capacities to improve MSCs *in situ* transfection with a reduced cytotoxicity. *In situ* chondrogenesis of hMSCs inside G-HACG P80PX was achieved using a plasmid encoding for the transcription factor SOX9 (p*sox9*), leading to effective chondrogenic differentiation with reduced expression of fibrocartilage and hypertrophic markers [14]. The potential of the developed systems to restore cartilage extracellular matrix was lastly confirmed in an *ex vivo* model of chondral defect.

2. Materials and methods

2.1. Materials

All reagents were obtained from Gibco-ThermoFisher Scientific (Madrid, Spain) except where otherwise indicated. Hyaluronic acid sodium salt (MW 1.38 MDa), *N,N,N′,N′*-Tetramethylethylenediamine (TEMED, 99%), Polysorbate 80 (Tween 80, 1,311.7 g/mol, HLB 14.9), Dimethyl-Methylene Blue Dye (DMMB), L-Cysteine, paraformaldehyde (37% *v*/v), DNA standard solution, Toluidine blue, recombinant TGF-β3 (TGF-β3), Methyl-beta-cyclodextrin, Dexamethasone, Sodium L-ascorbate, Sodium pyruvate solution (100 mM), Alizarin Red Solution and anti-type X collagen were purchased from Sigma Aldrich (St Louis, MO, USA). The anti-type II collagen (II-II6B3) antibody was purchased from DSHB (Iowa, IA, USA). The anti-SOX9 (E-9) and the anti-type I collagen (COL-1) were purchased from Santa Cruz Biotechnology (Heidelberg, Germany). The biotinylated secondary antibody (Ig G H + L) and the ABC and DAB reagents were obtained from Vector Laboratories (Alexis Deutschland GmbH, Grünberg, Germany). First Strand cDNA Synthesis Kit for RT-PCR and cell proliferation reagent WST-1 were purchased from Roche (Mannheim, Germany). The RNeasy Kit was from Qiagen (Hilden, Germany). The Safranin-O powder was from Carl Roth (Karlsruhe, Germany). 1,2-di-O-octadecenyl-3-trimethylammonium propane (chloride salt) (DOTMA, MW 670.575 g/mol) was obtained from Avanti Polar Lipids (Alabaster, AL, USA). The Beta-Glo Assay System and the Cell Culture Lysis 5× Reagent were purchased from Promega (Madison, WI, USA), and Chondroitin sulphate C was purchased from TRC (Toronto, ON, Canada). Equinox ™ Platinum Silicone was obtained from Smooth-On (Macungie, Pennsylvania, USA). Poloxamer 407 (PX; 14,600 g/mol, HLB 18-23) was kindly provided by BASF (Ludwigshafen, Germany). The p0DB-001_pEGFP-N1 (pGFP; bp 4733) and pACP-FLAG-hsox9 (p*sox9*, bp 6915) were kindly donated by Dr. Romero-Saavedra and Prof. M. Cucchiarini, respectively.

2.2. Production of non-viral vectors

2.2.1. Plasmid isolation and purification

Plasmids encoding for β-galactosidase (p*lacZ*), green fluorescent protein (pGFP), and SOX9 (p*sox9*) were propagated, purified, and quantified following standard procedures [10]. All pDNA solutions were diluted to reach a concentration of 250 μg/ml and stored at −20°C until use.

2.2.2. Niosome preparation

Niosomes were synthesized by a modification of the thin film hydration technique [15]. Briefly, DOTMA (2 mg, 0.40 ml), polysorbate 80 (P80; 7.5 mg, 0.05 ml), poloxamer 407 (PX; 7.5 mg, 0.05 ml) and cholesterol (5 mg, 0.15 ml) were dissolved in dichloromethane and the organic solvent was removed under argon flow. The obtained lipid film was hydrated with 3 ml of OptiMEM medium and sonified for 30 s at 40% amplitude using a UP200S Sonifier (Hielscher Ultrasound Technology, Germany) with a 2 mm probe. The final DOTMA concentration obtained in the niosome dispersions was 600 ng/ml.

2.2.3. Characterization of nioplexes

Nioplexes were formed by mixing the appropriate amounts of plasmid (0.1 μg for p*lacZ* or 1 μg for pGFP and p*sox9*) and niosome solution (P80PX, 600 ng/ml) to obtain 2.5/1, 5/1, 10/1, 15/1 and 20/1 cationic lipid/DNA mass ratio, corresponding to 1, 2, 5, 7 and 10 nitrogenous (N) to phosphorus (P) ratios. All samples were allowed to complex for 30 min at room temperature before being used in different experiments [9,10]. Lipoplexes formed with Lipofectamine were used as positive control and prepared by mixing equal amounts of plasmids and the recommended reagent volume according to the manufacturer's instructions.

2.2.3.1. Particle size, zeta potential, and morphology evaluation (TEM). The particle size and zeta potential of nioplexes were measured at room temperature using Dynamic Light Scattering (DLS) and Electrophoretic Light Scattering (ELS) with a NanoBrook 90Plus Zeta (Brookhaven Instruments Corporation, Holtsville, NY, USA). The samples were prepared by diluting 150 μl of nioplexe solutions obtained as described in Section 2.2.3 in 1.5 ml of OptiMEM medium [15]. Measurements were performed by triplicate.

Morphology of P80PX niosomes was evaluated by placing 5 μl of niosome stock on carbon-coated grids. Samples were observed using a high-resolution JEM-1010 TEM (JEOL USA Inc., Peabody, MA, USA).

2.2.3.2. Capacity of DNA protection. The capacity of the proposed niosome formulations to protect DNA was evaluated by agarose gel electrophoresis assay [10]. For the electrophoresis assay, naked p*lacZ* (control) or p*lacZ* (0.1 μg) nioplexes (prepared as described in Section 2.2.3) were incubated at 37°C for 30 min in the presence of DNase (2.5

μg DNA/ U DNase) and run in an agarose gel (0.8% in TBE) exposed for 45 min to 90 V. DNA bands were stained with SYBR Green (0.05% in TBE), and images were observed under a digital Chemi-Doc™ Imaging System (Bio-Rad, Madrid, Spain) [10].

2.3. Cytotoxicity and transfection efficiency of nioplexes

2.3.1. Isolation and culture of human bone marrow-derived mesenchymal stem cells (hMSCs)

Bone marrow aspirates were obtained from the distal femurs of patients undergoing total knee arthroplasty ($n = 8$). The study was approved by the Comité de Ética de Investigación da Coruña (accession number: 2019/066). All patients provided their informed consent prior to inclusion in the study. All procedures were executed in compliance with the Helsinki Declaration. hMSCs were isolated and expanded in culture using standard protocols and characterized for MSC-positive surface markers [10]. Cells were kept in Dulbecco's Modified Eagle Medium (DMEM), 10% Fetal Bovine Serum (FBS), 1% Penicillin/ Streptomycin (P/S) (supplemented medium), and used at passages 1–3 in all experiments.

2.3.2. Cytotoxicity evaluation and placZ expression in hMSCs

The hMSCs were seeded in 96 well-plates at an initial density of 6400 cells/cm^2 and allowed to attach for 24 h at 37°C before the experiments. Cells were exposed to nioplexes formed as described in Section 2.2.3. hMSCs cultured without nioplexes and cells transfected with the commercial reagent Lipofectamine (LPF; 0.4 μl/well) were used as negative and positive controls, respectively. Cells were incubated with lipo- or nioplexes for 24 h at 37°C and 5% CO_2 prior to viability and transfection evaluation. All conditions were assessed by triplicate.

Viability of the hMSC monolayers was monitored using the WST-1 method, following the manufacturer's instructions. The absorbance (Abs) signal at 450 nm was measured in a Sinergy HTX Plate reader (Biotek, Winooski, USA). Cell viability was calculated following eq. 1.

$$Cell\ viability\ (\%) = \frac{Abs\ sample_{450\ nm}}{Abs\ control_{450\ nm}}\ x\ 100 \quad (1)$$

The transfection efficiency of hMSCs achieved with p*lacZ* nioplexes was evaluated by using the β-glo reagent. Cells were washed with PBS and lysed with 110 μl/well of Cell Culture Lysis Reagent (1:50 *v*/v). Then, 50 μl of cell lysates were added to 50 μl of β-glo reagent, and luminescence was measured by means of a plate reader. Endogenous β-galactosidase activity recorded for the negative control was used as a blank and subtracted for each condition. All values were normalized to the total protein content quantified using a BCA kit following the manufactures instructions [10].

2.3.3. Internalization mechanism of nioplexes

The endocytosis mechanisms of nioplexes were analysed by measuring the β-galactosidase after treatment with various endocytosis inhibitors. The hMSCs were plated in 96-well plates at 6,400 cells/cm^2 and incubated for 24 h. Chlorpromazine (CHL, clathrin-mediated endocytosis inhibitor, 30 μM, 1 h), genistein (GEN, caveolae-mediated endocytosis inhibitor, 200 μM, 1 h), methyl-β-cyclodextrin (MβC, clathrin- and caveolae-dependent endocytosis inhibitor, 2 mM, 10 min), and amiloride (AMI, macropinocytosis inhibitor, 5 mM, 10 min) were added per triplicate and incubated with cells at the denoted conditions before transfection with nioplexes (5/1 cationic lipid/DNA ratio) for 4 h. Control conditions included untransfected cells and cells transfected in absence of inhibitors. β-galactosidase activity and cell viability were measured following the same protocols described in Section 2.3.2 [10].

2.4. Preparation of hyaluronic acid-based cryogels (HACGs)

2.4.1. Production of methacrylated hyaluronic acid (MetHA)

MetHA was synthesized and purified using a modified protocol for high molecular weight HA methacrylation [12]. Briefly, 500 mg of HA was dissolved under magnetic stirring in 80 ml PBS at 4°C for 12–16 h. Then, the mixture was cooled down in an ice-water bath and 30 ml of dimethylformamide (DMF) were added in a dropwise manner. The reaction was left at room temperature before glycidyl methacrylate (GM, 5.6 g, 5.3 ml) and triethylamine (TEA, 2.8 g, 4 ml) were added. The solution was stirred at room temperature and protected from light for 7 days. The mixture was then purified by dialysis (Biotech 100 kDa membrane) for 5 days and freeze-dried using a Cryodos −80°C Lyophilizer (Telstar, Madrid, Spain) for 48 h. Resulting MetHA product was solved in D_2O, analysed by ^{1}H-RMN (Varian, 500 MHz), and the percentage of methacrylation was determined by analysing the H-RMN spectra, according to eq. 2 [16].

$$Methacrylation(\%) = \frac{I\ (MetHA)}{I(MetHA + HA) - I(MetHA)}\ x\ 100 \quad (2)$$

Where, I (MetHA) represents the intensity of the peak corresponding to the methyl group next to the alkene (~1.7 ppm) and I (MetHA + HA) the intensity of the peak corresponding to both methyl groups, one next to the alkene and the other next to the ketone (~1.9 ppm).

2.4.2. Production and characterization of HACGs

The HACGs were synthesized by redox-induced free-radical polymerization of MetHA. The MetHA was dissolved in deionized water and cooled down at 4°C for 24 h. HACGs were prepared by mixing 100 μl of MetHA solution (5% *w/v*) with 10 μl of APS (40 μg/μl) and 10 μl of TEMED (70 μg/μl) per well (4 or 6 mm-diameter) in a pre-cooled handmade platinum-silicone mold (4°C). The mixture was then placed at −20°C and froze within a minute. After an incubation of 24 h, the gels were gradually warmed first in an ice bath, next at 4°C and then at room temperature to remove ice crystals and extensively washed with deionized water for 5 days [12].

2.4.2.1. Swelling ratio measurements. Swelling kinetics of the HACGs were conducted following conventional gravimetric procedure [11]. Freeze-dried cryogel samples ($n = 3$, 1 mm × 6 mm) were weighed and then placed in PBS for 2 h until swelling equilibrium was reached. The swelling ratio was determined by eq. 3.

$$Swelling\ (\%) = \frac{W_s - W_d}{W_d} \quad (3)$$

Where, W_s and W_d are the weights of the swollen and dried cryogel samples, respectively.

2.4.2.2. Biodegradation assays. The dried HACGs specimens ($n = 3$, 1 mm × 6 mm) were weighed, sterilized in ethanol (70% *v*/v), and washed with culture medium until swelling equilibrium. Sterilized scaffolds were then transferred to a 12-well plate filled with PBS, alone or containing 250 U/ml hyaluronidase, and incubated at 37°C for 28 days. Then, samples were collected at regular intervals, dried, and weighed again. The degree of biodegradation was determined using the following eq. 4 [11,17].

$$Degree\ of\ degradation\ (\%) = \frac{W_1 - W_2}{W_1} \quad (4)$$

Where, W_1 and W_2 correspond to the weight of cryogel samples at the initial and denoted final time points, respectively.

2.4.2.3. Scanning electron microscopy. Freeze-dried HACGs samples ($n = 2$, 1 mm × 6 mm) were coated with gold and imaged using secondary electron detection on a JEOL JSM-6400 Scanning Electron Microscope (JEOL USA Inc., Peabody, MA, USA) at 15 kV. Porosity percentages and pore sizes were determined in triplicate in 3 different specimens using ImageJ software [18].

The hMSCs were seeded in cryogel sections (1 mm × 6 mm), fixed in

glutaraldehyde 2.5% for 3 h at room temperature, dehydrated in an increasing concentration gradient of ethanol, dried in a critical point dryer, coated with gold and finally imaged on a Scanning Electron Microscope [18].

2.4.2.4. Porosity. Freeze-dried cryogel samples ($n = 3$, 1 mm × 6 mm) were weighed, incubated in ethanol (1 ml, 30 min), wiped, and weighed again. The percentage of porosity of the scaffolds was determined following eq. 5 [11].

$$Porosity\ (\%) = \frac{(W_2 - W_3 - W_s)/\rho_e}{(W_1 - W_3)/\rho_e} \quad (5)$$

Where W_1 represents the weight of the vial filled with ethanol, W_2 the weight of the bottle weight including ethanol and cryogel samples, W_3 the weight of the vial measured after taking out ethanol-saturated cryogel, W_s the weight of ethanol-saturated cryogel samples and ρe the density of ethanol.

2.4.2.5. Shape memory test. The shape memory behaviour of the developed scaffolds was determined by comparing the weight of the hydrated cryogels before and after lyophilization. Briefly, cryogel samples ($n = 3$, 1 mm × 6 mm) were incubated for 2 h in PBS and weighed. The samples were freeze-dried, rehydrated under the same conditions, and weighed again. The shape memory ability of cryogels was determined following eq. 6.

$$Shape\ memory\ (\%) = \frac{W_i}{W_f}\ x\ 100 \quad (6)$$

Where, W_i and W_f are the weights of the hydrated cryogel samples before and after lyophilization, respectively [11].

2.4.2.6. Rheological measurements. Freeze-dried and hydrated HACGs samples were analysed on a Hybrid Discovery HR-2 Rheometer (TA Instruments, USA) at room (25°C) and body temperature (37°C). In all cases, cryogel samples ($n = 3$, 1 mm × 6 mm) were placed on a parallel plate stainless steel geometry with a gap width of 500 μm, plate diameter of 40 mm, and subjected to a constant strain of 0.1 N. The storage modulus (G'), the loss modulus (G"), and phase angle were calculated using an oscillatory logarithmic sweep at an increasing frequency between 0.1 Hz and 10 Hz [19].

2.4.2.7. Incorporation of nioplexes into HACGs, pDNA release profile, and bioactivity determination. Previous to the incorporation of nioplexes and lipoplexes within the HACGs, the cytotoxicity profile of sucrose, selected as pDNA cryoprotectant agent for freeze-drying [20], was tested by applying an increasing gradient from 0 to 100 mM sucrose in OptiMEM to hMSC monolayers. Cell viability was determined as described in Section 2.3.2. Based on these assays a 30 mM sucrose concentration was chosen for the following assays.

Freeze-dried HACGs samples (1 mm × 4 mm) were loaded with 50 μl of P80PX nioplexes (5/1 DOTMA/DNA mass ratio) or lipoplexes (LPF, positive control) in a dropwise manner (1 μg of plasmid) in the presence of 30 mM sucrose. Control conditions included HACGs loaded with the same complexes in the absence of sucrose. The loaded HACGs samples were then incubated overnight in 300 μl of PBS at 4°C [21] and incubated at 37°C (controls; P80PX and LPF). Half of the samples were freeze-dried again, rehydrated in 300 μl of PBS, and incubated at 37°C (P80PX or LPF 30 mM sucrose). All conditions were evaluated in triplicate.

At fixed time intervals (0.2, 1, 7, 14, and 21 days), aliquots of PBS medium were collected, immediately frozen at −20°C, and replaced with a similar volume (300 μl) of fresh medium. After 21 days, cryogels were digested in 500 μl of papain solution (10 mg/ml) overnight and stored at −20°C until processing. The amounts of pDNA released from HACGs samples in collected aliquots or retained into the matrices were quantified by Hoechst 33342 previous decomplexation of nioplexes or lipoplexes by incubating the samples with 3% SDS [20]. Fluorescence intensities ($\lambda_{exc} = 360$ nm, $\lambda_{em} = 485$ nm) were measured using a plate reader.

Bioactivity of the pDNA released *via* nioplexes and lipoplexes from HACGs was assessed at the denoted time points by placing aliquots of released medium (50 μl) in contact with hMSC monolayers seeded in the same conditions described in Section 2.3.2. [22]. After 24 h β-galactosidase activity and cell viability of the different conditions were evaluated as described in Section 2.3.2.

2.5. Production of gene activated hyaluronic acid-based cryogels (G-HACGs)

Freeze-dried HACGs (1 mm × 4 mm) were loaded with an appropriate volume of P80PX nioplexes or LPF lipoplexes (1 μg of pGFP, final volume 50 μl) in the presence of 30 mM sucrose as described in Section 2.4.2.7. Loaded HACG samples were subsequently freeze-dried and rehydrated with hMSCs cell suspension (10^6 cells; 20 μl) to obtain G-HACGs. The G-HACGs were incubated for 3 h prior to the addition of 300 μl of DMEM (10% FBS, 1%P/S). The HACGs samples loaded with P80PX nioplexes and cells (G-HACGs) were analysed by SEM following the same procedure described in Section 2.4.2.3.

2.5.1. Cytotoxicity evaluation and in situ transfection efficiency

After 48 h incubation, G-HACG samples were visualized with an AR1 confocal microscopy (Nikon, Tokyo, Japan). The efficiency of pGFP transfection was calculated using ImageJ software by counting GFP-positive cells relative to the total number of cells (%) in three standardized sections per sample. The viability of GFP-transfected cells was calculated by comparing the cell number per sample relative to the number of cells in the untransfected control [10].

2.6. Chondrogenesis of hMSCs in G-HACGs in situ and in an ex vivo model of chondral defect

The HACGs were freeze-dried and loaded with an appropriate volume of p*sox9* P80PX nioplexes or LPF lipoplexes, prepared as described in Section 2.2.3. (1 μg of plasmid, final volume 50 μl) and subsequently freeze-dried. G-HACGs were obtained by rehydration of loaded HACGs with hMSCs cell suspension (10^6 cells; 20 μl) following the same procedure described in Section 2.4.2.7.

Osteochondral (OC) plugs were generated from the tibial saucers of donor patients undergoing total knee arthroplasty ($n = 4$). The study was approved by the Comité de Ética de Investigación da Coruña (accession number: 2019/066). All patients provided their informed consent prior to inclusion in the study. All procedures were executed in compliance with the Helsinki Declaration.

The groups included HACGs loaded with nioplexes (G-HACG P80PX) or LPF lipoplexes (G-HACG LPF) and seeded with hMSCs, cryogels seeded with hMSCs in the absence of non-viral vectors (HACG (+)) and empty cryogels (HACG (−)). All conditions were evaluated in duplicate.

Osteochondral plugs ($n = 8$) were extracted using a Φ 8 mm Arthrex OATS Biopsy bone extruder (Arthrex, Naples, FL, USA) under sterile conditions. Each OC plug was washed with PBS, transferred to a 24-well plate and a focal defect of 4 mm diameter was created at the center using a biopsy punch [23]. The removed tissue was then discarded, and the defect was filled with the corresponding cryogel group.

Both G-HACGs or HACGs (*in situ* transfection) and explants filled with G-HACGs or HACGs (*ex vivo* defect model) were incubated in defined chondrogenic medium (DMEM, 0.1 μM dexamethasone, 50 μg/ml ascorbic acid, 110 μg/ml sodium pyruvate, 6.25 μg/ml insulin, 6.25 μg/ml transferrin, 6.25 μg/ml selenious acid, 10 ng/ml TGF-β3) [10] for 21 and 28 days, respectively.

2.6.1. Biochemical analysis

Before digestion, bone tissue was cut with a surgical blade from OC explants. Cryogels (HACG (+), G-HACG P80PX and G-HACG LPF) and chondral plugs filled with cryogels (HACG (+), G-HACG P80PX and G-HACG LPF) were longitudinally cut in 2 halves. One half was used for biochemical assays and the other half for RT-PCR analysis. Samples were digested in papain (10 mg/ml, pH 6.5) at 60°C for 2 h until complete dissolution of cryogel and cartilage tissue. The proteoglycan contents were quantified by complexation to dimethylmethylene blue dye (DMMB) [10]. Absorbance measurements at 595 nm were performed in a plate reader using chondroitin sulfate as standard. All measurements were performed by triplicate. Data were normalized to the total protein content calculated as in Section 2.3.2.

2.6.2. Histological and immunohistochemical analyses

Cryogels (HACG (−), HACG (+), G-HACG P80PX and G-HACG LPF) and OC plugs filled with cryogels (HACG (+), G-HACG P80PX and G-HACG LPF) were fixed in paraformaldehyde (4% *v*/v, 40 mg/ml sucrose and 10 μl/ml of 1 M NaOH) for 4 h. After washing in PBS, cryogels and OC plugs were embedded in a block with melted agarose (3% *w/v*). Once the agarose was cooled, the blocks were transversally cut using a motorized vibroslice tissue slicer (NVSLM1-363, WPI) [24]. Sections ranging 100 μm in thickness were taken from the vibrating microtome with a thin paintbrush and placed in 24-well plates with 1× PBS.

To evaluate the cellularity of HACG (+), G-HACG P80PX, and G-HACG LPF, sections were permeabilized with Triton X-100 (0.2% in PBS) for 5 min at room temperature. Then, DAPI (300 nM in PBS) was added and incubated for 5 min at room temperature. Finally, samples were washed 2 times with PBS and observed under a fluorescence inverted microscope Olympus CKX53 [9].

The HACG (−), HACG (+), G-HACG P80PX, and G-HACG LPF sections were stained with Toluidine Blue (matrix proteoglycans) and Alizarin Red (calcium deposits) following standard procedures [10], while cartilage defects filled with HACGs (+), G-HACG P80PX and G-HACG LPF were stained with Safranin-O/Fast Green for proteoglycans assessment [23].

In all groups of study expression of SOX9, type-I, type-II, and type-X collagen was evaluated by immunohistochemistry using specific antibodies, biotinylated secondary antibodies, and the ABC method with diaminobenzidine as the chromogen for both *in situ* and *ex vivo* models [10]. All samples were examined under light microscopy (Olympus CKX53).

Histomorphometric analysis was performed at three random standardized sites for condition and replicate using the ImageJ software. Background staining from empty cryogels (HACG (−)) was used as blank and subtracted for each condition and group of study.

2.6.3. Total RNA extraction and real-time RT-PCR analyses

Cryogels and chondral plugs filled with cryogels samples (same groups described in Section 2.6.1) were digested with TRIzol Reagent and chloroform and precipitated with ethanol (70% *v*/v). For chondral plugs, an additional mechanical rupture was applied using 5 cycles of 3 min at a frequency of 2.5 Hz in a MM200 Tissue Homogenizer (RETSCH, Biometa Technology and Systems, Asturias, Spain). RNA was purified using an RNase extraction kit following the manufacturer's instructions.

Reverse transcription was carried out with 8.2 μl of eluate using the 1st Strand cDNA Synthesis kit for RT-PCR (AMV) and 3 μl of cDNA product was amplified with real-time PCR using the Power Up SYBR Green Master Mix on a QuantStudio3 qPCR operator (ThermoFisher, Madrid, Spain) under the following conditions: Hold stage (50°C, 2 min), denaturation (95°C, 2 min), amplification by 40 cycles (denaturation at 95°C, 15 s; annealing/extension at 60°C, 1 min). Melt curve stage was recorded under the next conditions: denaturation (95°C, 5 s), annealing/extension (65°C, 10 s, temperature gradient of 1.6°C/s) and dissociation (95°C, 1 s, temperature gradient of 0.5°C/s). The primers (ThermoFisher, Madrid, Spain) used [10] were aggrecan (ACAN, chondrogenic marker for proteoglycans) (F 5'-GAGATGGAGGGT-GAGGTC-3′; R 5'-ACGCTGCCTCGGGCTTC-3′), SOX9 (early chondrogenic transcription factor) (F 5′-ACACACAGCTCACTCGACCTTG-3′; R 5'-GGGAATTCTGGTTGGTCCTCT-3′), type-II collagen (COLII, chondrogenic and matrix marker) (F 5′-GGACTTTTCTCCCCTCTCT-3; R 5′-GACCCGAAGGTCTTACAGGA-3′), type-I collagen (COLI, osteogenic marker) (F 5′-ACGTCCTGGTGAAGTTGGTC-3′; R 5′-ACCAGG-GAAGCCTCTCTCTC-3′), type-X collagen (COLX, marker of hypertrophy) (F 5′-CCCTCTTGTTAGTGCCAACC-3′; R 5′-AGATTC-CAGTCCTTGGGTCA-3′), and mitochondrial 18S ribosomal RNA (RNN18s, housekeeping) (F 5′-GAAGGTGAAGGTCGGAGTC-3′; R 5′-GAAGATGGTGATGGGATTTC-3′). The threshold cycle (Ct) value for each gene of interest was measured for each amplified sample by using the QuantStudio software. Both, RRN18s and the control group (HACG (+) and chondral plug filled with HACG (+) values were used to calculate the gene expression of each sample using the $2^{-\Delta\Delta Ct}$ method, as previously described [10].

2.7. Statistical analyses

Statistical analysis was performed by parametric (one-way ANOVA; Student's *t*-test) and non-parametric test (Kruskal-Wallis, U-Mann Whitney) using IBM SPSS Statistics *v23* software. Final values were expressed as mean ± standard deviation (SD). A $p \leq 0.05$ was considered statistically significant.

3. Results

3.1. Production of non-viral vectors

Niosomes composed by DOTMA, P80, PX, and cholesterol were synthesized by a modification of the thin-film hydration technique. After mixing with a proper volume of p*lacZ*, the niosomes and the resulting nioplexes were characterized in terms of size, polydispersity, and zeta potential (Fig. 1A and Table TS1). The mean size, polydispersity index (PDI), and zeta potential values measured for P80PX niosomes blank (**N**) were 204.8 ± 6.8 nm, 0.22 ± 0.01, and 26.5 ± 4.6 mV, respectively. Representative TEM figures are shown in Fig. S1.

Complexation of p*lacZ* with P80PX formulations led to a significant reduction of nioplexes sizes, leading those nioplexes formed at 20/1 DOTMA/DNA ratio to the lowest sizes (266.6 ± 30.8 *versus* 431.7 ± 4.5 nm for the nioplexes formed at 2.5/1 and 20/1 DOTMA/DNA ratios, respectively $p = 0.006$). In contrast, the smallest values of PDI were observed at the lowest DOTMA/DNA values (2.5/1), being similar to those measured for niosomes (~0.23; $p = 0.393$).

When studying the zeta potential of the nioplexes a gradual increase in electropositivity was evidenced by increasing the DOTMA/DNA ratio, with the highest difference at the greater ratio (20/1) tested (up to 17.3 times difference when comparing with 2.5/1 DOTMADNA ratio; $p = 0.002$).

The DNase protection assay (Fig. 1B) was used to investigate the capacity of the developed niosome formulation to protect the plasmid from the degradation of microenvironment enzymes. In contrast to that observed with free plasmid (0) that resulted in a total degradation, an increased protection ability of the nioplexes was noted with the increase of the DOTMA/DNA ratio from 2.5/1 to 20/1 exhibiting the SC (supercoiled) and OC (open circular) bands corresponding to the active form of the plasmid.

3.2. Cytotoxicity and transfection efficiency of nioplexes

Fig. 2A depicts the transfection efficiency and cytocompatibility of P80PX nioplexes upon contact with hMSC monolayers. The highest transfection efficiency of the P80PX nioplexes was achieved in an intermediate DOTMA/DNA ratio of 5/1, which led to a 17.3-fold increase on β-galactosidase activity compared to the rest of DOTMA/DNA ratios;

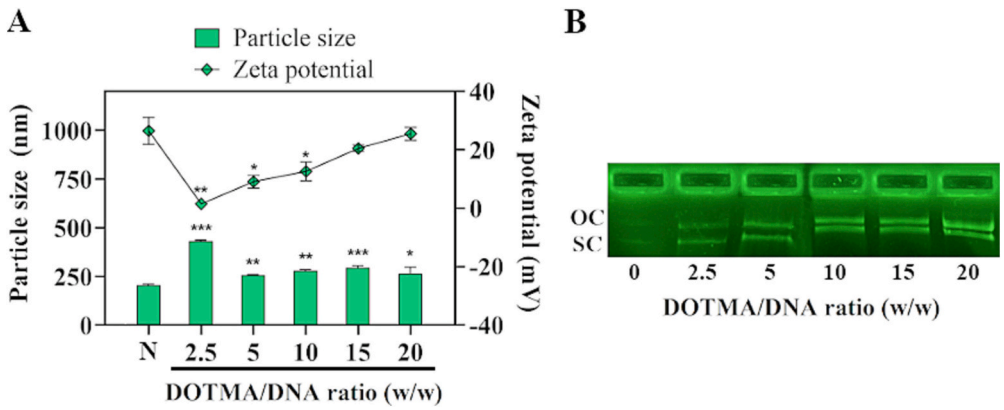

Fig. 1. Characterization of P80PX niosomes (N) and nioplexes formed at 2.5/1, 5/1, 10/1, 15/1, and 20/1 DOTMA/DNA ratios (**A**) Particle size and zeta potential measurements and (**B**) DNase protection ability assay. 0: naked p*lacZ*; OC: open circular; SC: supercoiled. *depicts $p < 0.05$, ** $p < 0.01$, and *** $p < 0.001$ when compared with 0 DOTMA/DNA ratio.

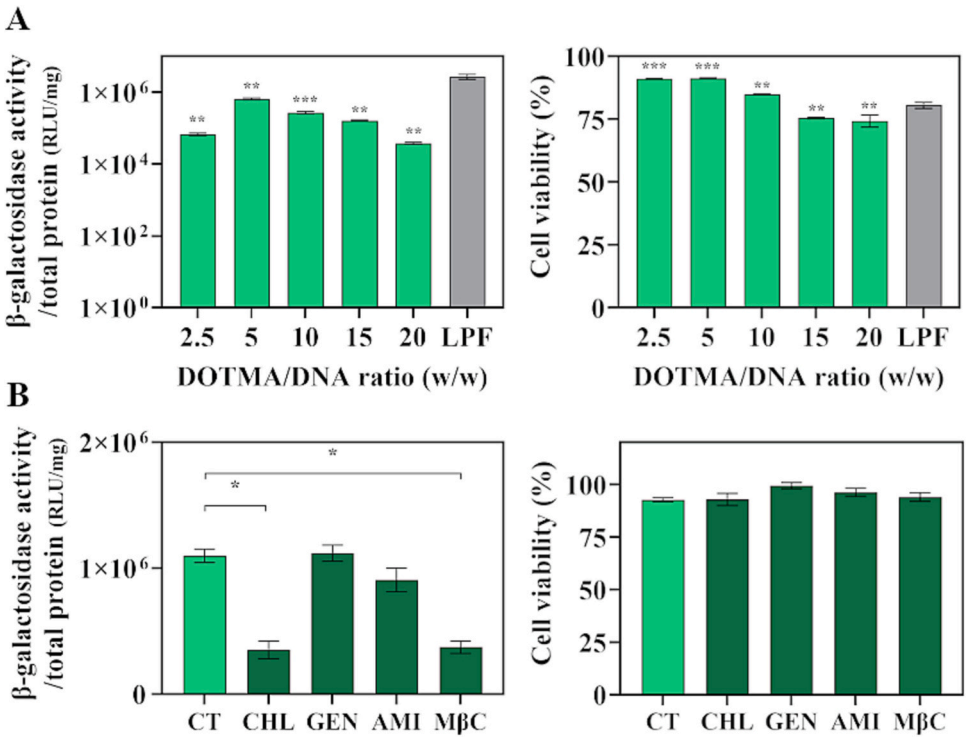

Fig. 2. *In vitro* transfection of hMSC monolayers with p*lacZ via* P80PX nioplexes (light green) formed at 2.5/1, 5/1, 10/1, 15/1, and 20/1 (up) or 5/1 DOTMA/DNA ratios (down). Samples were analysed for (**A**) β-galactosidase activity normalized to the total protein content (left) and cell viability (right) **represent $p < 0.01$ and *** $p < 0.001$, when compared with positive control Lipofectamine (LPF, grey). (**B**) β-galactosidase activity normalized to the total protein content (left) and cell viability (right) after pre-treatment with chlorpromazine (CHL), genistein (GEN), methyl-β-cyclodextrin (MβC) or amiloride (AMI). Control conditions included cells transfected in absence of inhibitor (control, CT, clear green). *depicts $p < 0.05$, when compared with denoted CT group. (For interpretation of the references to colour in this figure legend, the reader is referred to the web version of this article.)

$p < 0.01$). However, the transfection efficiency of the proposed nioplexes (655,669 ± 42,175 RLU/mg) was significantly lower than that achieved with the commercial reagent LPF (2,711,124 ± 440,861 RLU/mg, $p < 0.001$). It is noteworthy that the percentages of cell survival were markedly higher after transfection with P80PX nioplexes, especially used at 5/1 DOTMA/DNA ratio (~91%), than with the commercial reagent ($p < 0.001$).

To ascertain the endocytosis pathway of 5/1 DOTMA/DNA ratio P80PX nioplexes, we evaluated the expression of the *lacZ* transgene after treatment with a battery of different endocytosis inhibitors under optimized conditions [10] (Fig. 2B). A pronounced descent in the transfection signal was evidenced upon hMSCs pre-treatment with CHL (350,983 ± 69,742 RLU/mg) and MβC (371,781 ± 48,910 RLU/mg) compared with the untreated control (1,099,556 ± 53,034 RLU/mg); $p < 0.01$) confirming the preferential internalization of P80PX nioplexes by clathrin-mediated endocytosis.

3.3. Preparation of HACGs

For HACGs preparation, HA was first functionalized with methacrylate groups. ^{1}H NMR spectrum confirmed the presence of vinyl methylene peaks at 5.4 and 5.8 ppm, as a result of the incorporation of the methacrylate in the polymer structure, and also discarded the presence of unreacted glycidyl methacrylate in the final product. The degree of methacrylation (19 ± 4.8%) was estimated using eq. 2 comparing the intensities of the peaks at 1.8 and 1.9 ppm (Fig. S2), corresponding to the methyl peaks of MetHA and the precursor HA. To prepare HACGs, MetHA polymer was dissolved in high-purity water (5% *w/v*) and exposed to free radical cryopolymerization in platinum silicone molds to form macroporous scaffolds.

The HACGs showed a swelling ratio of 95.2 ± 1.2, shape-memory capacity of 98.2 ± 0.2%, and mean porosity of 98.2 ± 0.2% (Table TS2). As shown in Fig. 3 all the investigated cryogels displayed an interconnected macroporous structure with thick polymer walls. In

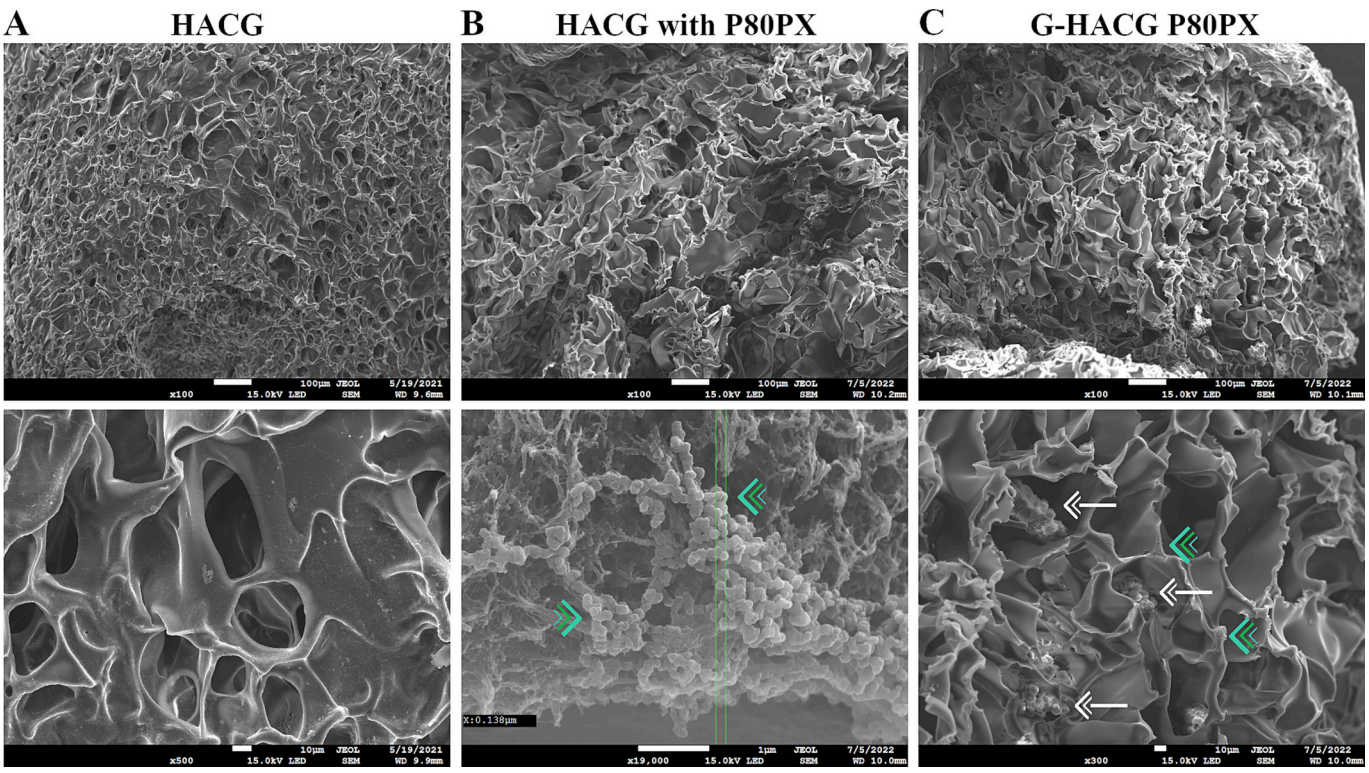

Fig. 3. SEM representative images of HACGs (**A**) solely (magnification 100× and 500×), (**B**) loaded with P80PX nioplexes (magnification 100× and 19,000×), or (**C**) loaded with P80PX nioplexes and hMSCs to obtain G-HACG (magnification 100×). P80PX nioplexes and hMSCs within the cryogels are pointed with green arrowheads and white arrows, respectively. (For interpretation of the references to colour in this figure legend, the reader is referred to the web version of this article.)

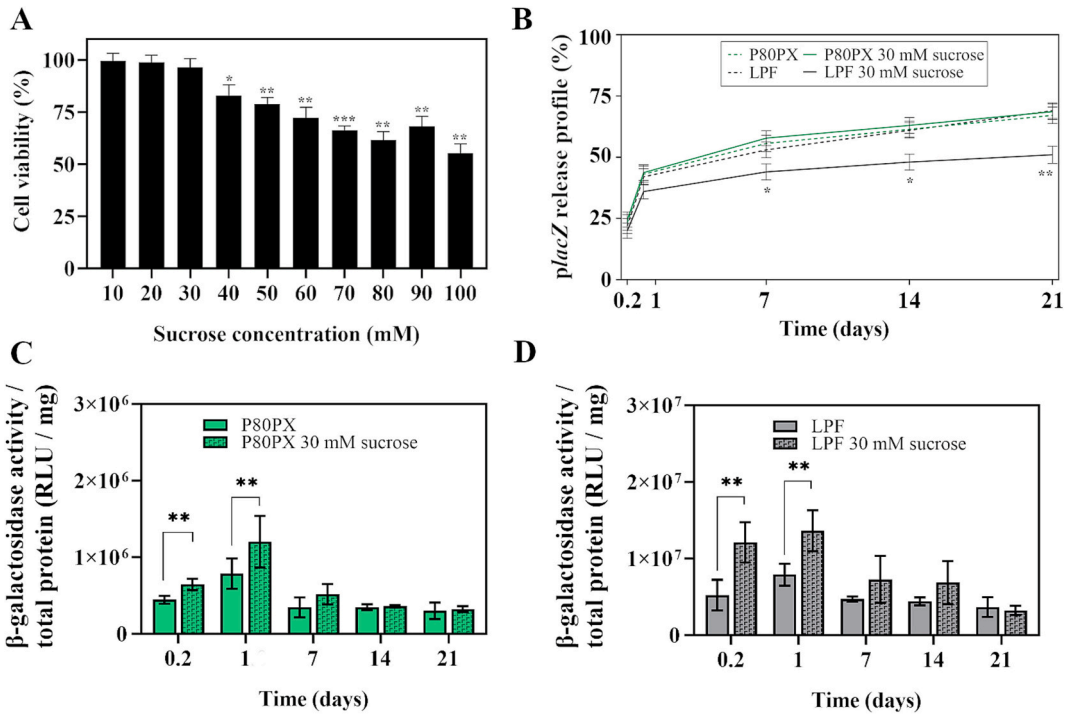

Fig. 4. Incorporation of P80PX nioplexes into HACGs. (**A**) Cytotoxic profile of sucrose (0–100 mM) in hMSC monolayers. (**B**) Cumulative release profiles of P80PX nioplexes (5/1 DOTMA/DNA ratio, green) and LPF lipoplexes (grey) directly loaded in freeze-dried HACGs cryogels or incorporated in freeze-dried HACGs cryogels and subsequently freeze-dried in presence of 30 mM sucrose, at 0.2, 1, 7, 14 and 21 days. Bioactivity of the pDNA released from (**C**) P80PX nioplexes (green) and **(D)** LPF lipoplexes (grey) at 0.2, 1, 7, 14, and 21 days represented as β-galactosidase activity normalized to the total protein contents. *represent $p < 0.05$, ** $p < 0.01$, and *** $p < 0.001$, when comparing freeze-dried (solid colour) and double freeze-dried (striped colour) groups. (For interpretation of the references to colour in this figure legend, the reader is referred to the web version of this article.)

agreement with gravimetric measurements, SEM images of HACGs revealed mean porosities of 90.5 ± 4.5% and pore size of 139.6 ± 15.2 μm. Moreover, the lyophilization steps necessary for the incorporation of the non-viral vectors (mean porosity 91.9 ± 2.9%, pore size 135.0 ± 5.0 μm; Table TS3**)** or incorporation of hMSCs (mean porosity 91.8 ± 2.1%, pore size 127.5 ± 6.5 μm; Table TS3) did not modify the properties of the scaffolds ($p \geq 0.05$).

Biodegradation profile of HACGs within 28 days is shown in Fig. S3. Cryogels showed a 42% of weight loss after 28 days and almost a 90% in presence of an optimized hyaluronidase dose [17] (Fig. S3). Rheology analyses of HACGs were performed at 25°C and 37°C in both dry and wet states. Fig. S4 shows the changes in G', G", and phase angle of cryogels with time. In the dry state, cryogels showed a stable G', showing that their elastic properties remained constant through the various forces applied over a period of time. The decrease in the G" and G' moduli and change in phase angle in the hydrated form indicates the flexibility of the cryogels changing from a stiff to soft spongy behaviour. The stabilization of the loss and storage moduli when reaching the swelling equilibrium indicates a fast water uptake, confirming the viscoelastic nature of the scaffolds.

3.4. Incorporation of nioplexes into HACGs, pDNA release profile, and bioactivity determination

For incorporation of the non-viral vectors into HACGs, a sucrose solution was added to the formulations of P80PX niosomes in order to maintain pDNA bioactivity during the freeze-drying step [20] (Fig. 3B). An evaluation of the cytotoxic profile of sucrose upon contact with hMSC monolayers showed high levels of cell viability when used at concentrations of up to 30 mM ($p \geq 0.13$ compared to untreated cells) (Fig. 4A). In contrast, a significant drop in cell survival was evidenced at concentrations higher than 40 mM, leading to a reduction by half at 100 mM ($p \leq 0.01$). Based on these results a 30 mM sucrose concentration was selected to incorporate the nioplexes into HACGs.

Fig. 4B shows the release profiles of p*lacZ*-based P80PX nioplexes (5/1 DOTMA/DNA ratio) directly loaded into HACGs (P80PX) or incorporated in presence of 30 mM sucrose and subsequently lyophilized (P80PX 30 mM sucrose). The same protocol was involved for the incorporation of LPF-based lipoplexes. The freeze-drying of HACGs with P80PX nioplexes did not modify their release showing superimposable profiles with ~60% of the pDNA released after 3 weeks. In contrast, freeze-drying of HACGs-containing lipoplexes significantly impacted their release profile showing a reduction in the p*lacZ* released after 21 days (51.0 ± 0.5% *versus* 69.0 ± 0.3%; $p < 0.001$). After 21 days, the percentage of pDNA retained in HACGs after digestion was ~23%, being lower with P80PX nioplexes than with LPF complexes ($p < 0.005$), in agreement with their higher release.

Next, we evaluated whether pDNA delivered from HACGs *via* nioplexes or lipoplexes was capable of transfection of MSC monolayers over time. In general, freeze-drying of HACGs containing P80PX nioplexes or LPF lipoplexes in presence of sucrose led to an increase of bioactivity of pDNA released (up to 2.0-fold in P80PX nioplexes and up to 2.3-fold in LPF lipoplexes, at 24 and 6 h, respectively; $p < 0.015$) (Fig. 4C and D).

3.5. Production of G-HACGs

Once loading P80PX nioplexes into HACGs we moved forward the incorporation of hMSCs to produce G-HACGs. SEM images obtained after loading the P80PX nioplexes into HACG demonstrated their retention inside the matrix (Fig. 3B) generating clusters around the cell aggregates (Fig. 3C).

In situ transfection of MSCs inside G-HACGs was evaluated by confocal microscopy of GFP expression (Fig. 5A) and quantified using ImageJ analysis software (Fig. 5B). When analysing the percentages of GFP positivity, G-HACG P80PX nioplexes achieved values similar to those achieved with G-HACG LPF lipoplexes (30.6 ± 2.8% and 39.1 ±

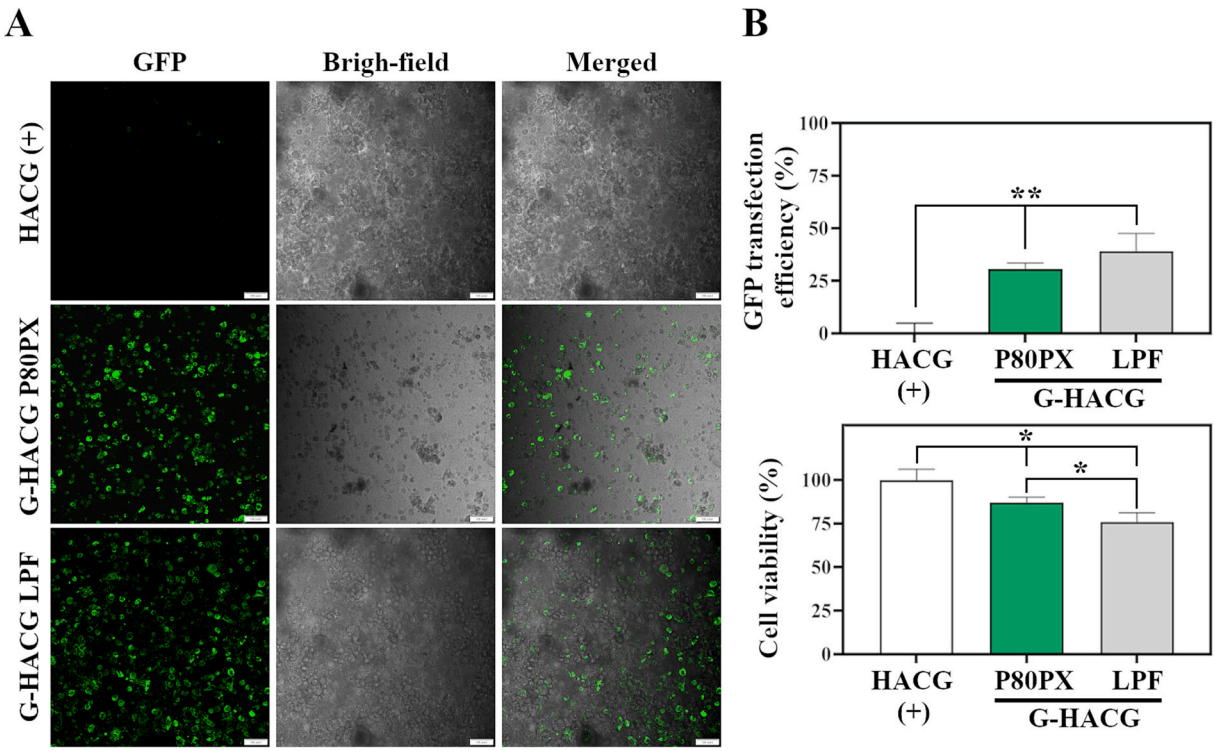

Fig. 5. *In situ* transfection of hMSCs seeded into HACGs (HACG (+), white) and transfected with pGFP *via* P80PX (5/1 DOTMA/DNA ratio, G-HACG P80PX, green) or LPF (G-HACG LPF, grey). Samples were cultured for 48 h and analysed by (**A**) Representative images of fluorescence microscopy showing GFP expression (scale bar 100 μm) and (**B**) Quantification of GFP transfection efficiency and cell viability as described in Materials and methods *represent $p < 0.05$ and ** $p < 0.01$, when comparing denoted groups. (For interpretation of the references to colour in this figure legend, the reader is referred to the web version of this article.)

8.5%, respectively, $p = 0.130$). Moreover, and similar to that observed in 2D transfection assays, cell survival in G-HACG P80PX was significantly higher than that achieved with G-HACG LPF (87.3 ± 2.9% *vs* 76.0 ± 5.3%, $p < 0.05$).

3.6. Chondrogenesis of hMSCs in G-HACGs in situ and in an ex vivo model of chondral defect

Once evaluated the potential of G-HACGs to promote MSCs *in situ* transfection while preserving cell viability, we tested their ability to induce hMSCs chondrogenesis by complexing P80PX niosomes with a plasmid encoding the transcription factor SOX9. Therefore, G-HACGs were loaded with P80PX nioplexes (G-HACG P80PX) or LPF lipoplexes (G-HACG LPF) and seeded with MSCs after a previous freeze-drying step. Empty HACGs (−) and HACGs (+) seeded with hMSCs in absence of non-viral vectors, were used as controls.

Cell numbers within HACGs after 21 days were assessed by DAPI staining (Fig. S5). In general, cell counts estimated for G-HACG groups were lower than those registered for HACG (+) group containing untransfected cells, but only G-HACG LPF group reached statistically significant differences compared with control ($p < 0.05$). Moreover, when comparing both G-HACG groups, a significant reduction in cell number was evidenced for G-HACG LPF ($p < 0.02$).

The *in situ* chondrogenesis of hMSCs was then evaluated by histological and immunohistochemical analyses (Fig. 6). An evaluation of SOX9 immunoreactivity showed mean values of pixels intensities of 115.7 ± 16.9 and 137.5 ± 11.3 for G-HACG P80PX nioplexes and G-HACG LPF lipoplexes, respectively, being significantly higher than those observed in HACG (+) control (76.4 ± 11.9; $p < 0.003$). A similar trend was observed for type-II collagen immunohistochemistry noting the highest immunoreactivity values in the G-HACG (up to 2.03-fold difference compared to the HACG (+) control; $p < 0.005$). However, no statistically significant differences between both G-HACG groups were reached ($p = 0.134$). An enhancement of Toluidine blue staining intensity was observed in G-HACGs compared with untransfected HACG (+) controls, especially in those containing P80PX nioplexes (up to a 1.75-fold increase compared with control; $p < 0.031$). These results were further confirmed by quantifying the proteoglycans amounts standardized to the total protein contents in the different cryogels groups (Fig. 7A), showing a higher deposition of proteoglycans in G-HACGs compared with HACG (+) controls (up to 2.30-fold increase; $p < 0.006$). According to the viability results, transfection *via* G-HACG LPF resulted in a reduction of protein contents (6.2 ± 0.8 μg) when compared to G-HACG P80PX (8.0 ± 0.5 μg) and HACG (+) control (8.7 ± 0.7 μg) ($p < 0.02$).

Of note, genetic modification of MSCs in G-HACGs led to a significant reduction in type-I collagen immunoreactivity, by 3 times compared with HACG (+) control and up to 4.0 times when compared with G-HACG LPF group ($p \leq 0.008$). A significant reduction in type-X immunoreactivity was also observed in G-HACG groups comprising P80PX in contrast with those containing LPF lipoplexes ($p = 0.002$). Moreover, *in situ* transfection of MSCs in G-HACG led to a reduction in Alizarin red staining compared with the untransfected HACG (+) control group ($p \leq 0.001$).

Histomorphometric and biochemical results were further corroborated by a gene expression analysis of relevant chondrogenic markers by real time RT-PCR (Fig. 7B). *In situ* transfection of hMSCs in G-HACGs led to an up-regulation of aggrecan and type-II collagen when compared

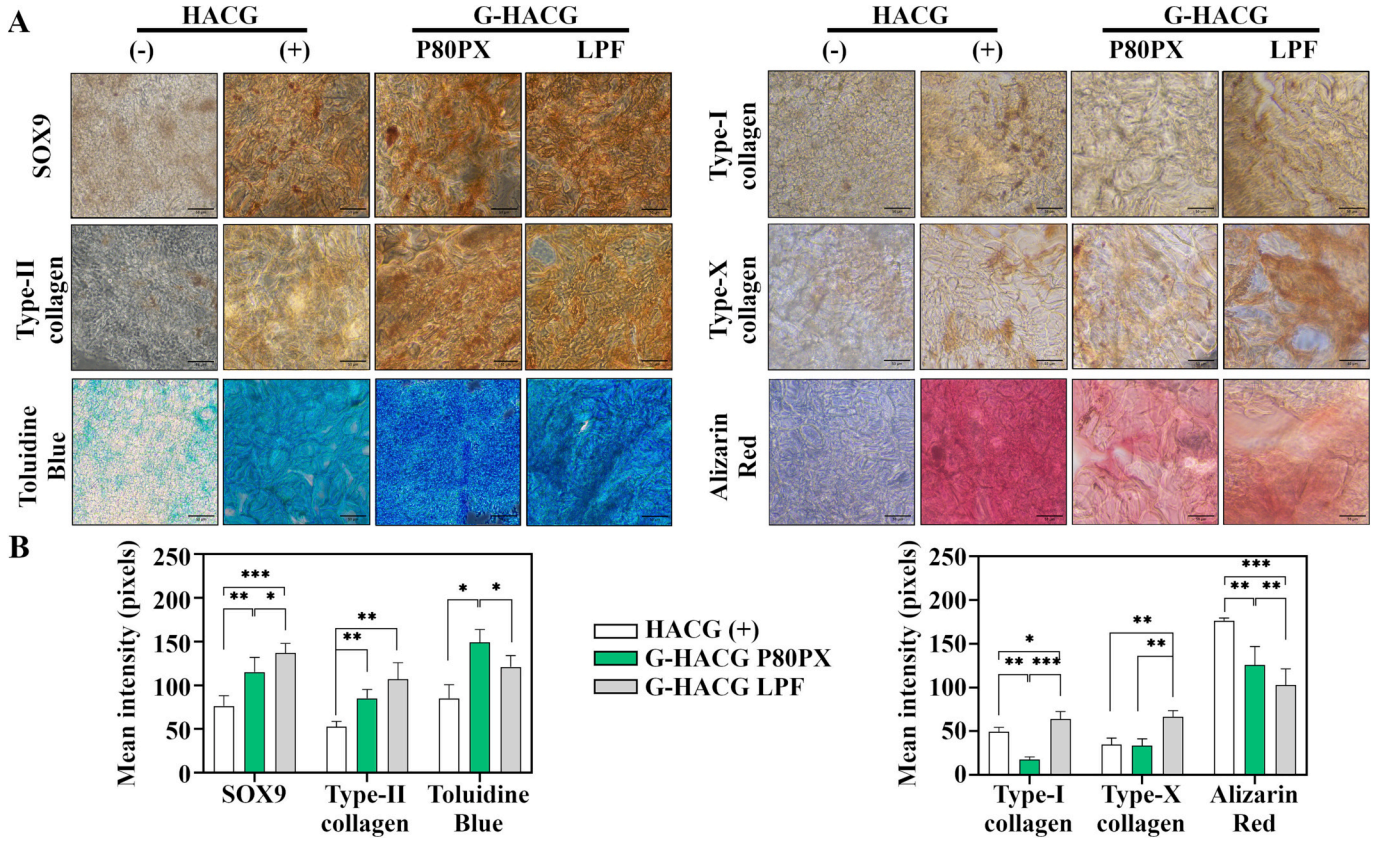

Fig. 6. *In situ* chondrogenesis of hMSCs seeded into HACGs and cultured in chondrogenic medium (HACG (+), white) and transfected with p*sox9 via* P80PX (G-HACG P80PX, green) or LPF (G-HACG LPF, grey). Samples were cultured in a chondrogenic medium for 21 days and processes for **(A)** histological and immunohistochemical analyses for immunodetection of SOX9, type-I, type-II, and type-X collagen, Toluidine blue and Alizarin red (scale bar 100 μm) and **(B)** histomorphometrical analysis realized as described in Materials and Methods (Section 2.6.2). *represent $p < 0.05$, ** $p < 0.01$ and *** $p < 0.001$, when comparing denoted groups. (For interpretation of the references to colour in this figure legend, the reader is referred to the web version of this article.)

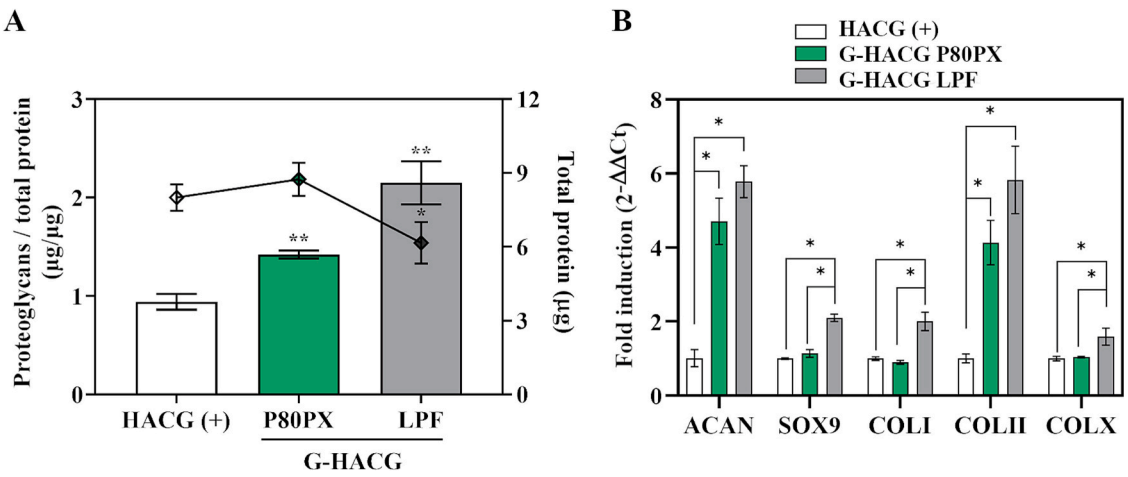

Fig. 7. *In situ* chondrogenesis of hMSCs seeded in HACGs and cultured in chondrogenic medium (HACG (+), white) and transfected with p*sox9 via* P80PX (G-HACG P80PX, green) or LPF (G-HACG LPF, grey). Samples were cultured in a chondrogenic medium for 21 days and processes for (**A**) proteoglycan contents standardized to the total protein contents and total protein contents and (**B**) Real-time RT-PCR analysis of aggrecan (ACAN), the transcription factor SOX9, type-I collagen (COLI), type-II collagen (COLII) and type-X collagen (COLX) with RRN18s serving as a housekeeping gene and internal control (primers are listed in Section 2.6.3). Ct values were obtained for each target, and fold inductions were measured by using the $2^{-\Delta\Delta Ct}$ method. *represent $p < 0.05$ when comparing denoted groups. (For interpretation of the references to colour in this figure legend, the reader is referred to the web version of this article.)

with HACG (+) control group (up to 6.0-fold increase; $p < 0.02$). In contrast, only G-HACG LPF group led to a statistically significant increase in SOX9 expression compared with HACG (+) control and G-HACG P80PX groups ($p < 0.03$). Lastly, only G-HACG LPF led to differences in type-I and type-X collagen compared with HACG (+) control ($p < 0.04$).

In order to evaluate the suitability of our systems from a preclinical perspective we moved on their testing in an *ex vivo* cartilage defect model (Fig. 8B). Lesions were filled with the different cryogels groups, cultivated for 28 days, and the grade of repaired tissue adjacent to the defects was studied by histological and immunohistochemical analyses (Fig. 8).

In agreement with Toluidine blue staining of G-HACGs (Fig. 6), an analysis of proteoglycans by Safranin-O staining in the immediately surrounding area to the defect, showed the highest intensities when filling the lesions with G-HACGs (up to 3-fold difference when comparing G-HACG P80PX with HACG (+) control group; $p < 0.004$) (Fig. 8A and C). These results were further confirmed by biochemical analysis, showing an increase in proteoglycans deposition when defects were filled with G-HACGs compared with those filled with untransfected controls (up to 2-fold difference; $p < 0.03$) (Fig. 9A). Additionally, a marked decrease on protein contents was evidenced in G-HACG LPF group ($p < 0.02$ compared with G-HACG P80PX and HACG (+)). Coincident outcomes were found for SOX9 and type-II collagen immunodetection, reaching the highest intensities when lesions were filled with G-HACGs, especially with those comprising P80PX nioplexes (Fig. 8A and C) ($p < 0.03$ compared with HACG (+) control). Lastly, and in good agreement with the immunohistochemical analysis of cryogels (Fig. 6), a significant reduction in hypertrophic and osteogenic markers was evidenced in the surrounding area of those lesions filled with G-HACG P80PX ($p < 0.04$ compared to G-HACG LPF or HACG (+) groups).

To determine the magnitude of these findings, a real-time RT-PCR assay was performed (Fig. 9B). Consistent with the histological analysis (Fig. 8) defects filled with G-HACGs showed an up-regulation of aggrecan, SOX9, and type-II collagen expression when compared with those lesions filled with untransfected HACG (+) control groups ($p \leq 0.04$) (Fig. 9B). Still, G-HACG LPF constructs exhibited a higher expression of these chondrogenic markers. Furthermore, in agreement with those analyses performed in isolated matrices (Fig. 7B), only the G-HACG LPF group led to statistically significant differences in type-I and type-X collagen expression compared to the untransfected HACG (+) control ($p \leq 0.04$).

4. Discussion

Gene-activated matrices have emerged as potential tools for tissue repair, offering the possibility of a spatiotemporal gene delivery, while promoting cell proliferation, differentiation, and matrix synthesis [6]. In the present study, *in situ* transfection of MSCs was achieved through their encapsulation inside a HA-based cryogel containing non-viral niosomal vectors. Further, MSCs gene transfer of the chondrogenic factor SOX9 inside these systems promoted the expression of hyaline-like cartilage markers in the adjacent zones of an experimentally created cartilage lesion.

Non-viral vectors based on niosomes have shown to be promising alternatives to classical liposomal formulations due to their improved chemical stability, lower cytotoxicity and feasibility of sterilization by autoclave [9]. Moreover, their ability to genetically modify MSCs and induce selective differentiation has been tested using pDNA that encodes chondrogenic factors [10].

The niosome formulations used in the present study comprise DOTMA as a cationic lipid, a blend of P80 and PX as non-ionic tensioactive agents, and cholesterol as a helper lipid. The rationality of choice of these compounds was based on our previous observations using niosome vectors to genetically modify MSCs leading to an effective transfection [9] while supporting high levels of cell viability [10].

It is well known that the uptake and transfection efficiency of nioplexes strongly depends on the size, superficial charge, and stability of the vectors [25]. Despite there is no general rule on the optimal physicochemical properties leading to high levels of transfection efficiency, the mean diameter of 200–300 nm, as those of the niosomes and nioplexes from the present study, seems to be appropriate for cell internalization [26]. As predicted, surface charge values of nioplexes gradually increased with the increment of positive charges donated by the cationic lipid, demonstrating their capacity to bind and neutralize the negative charges of the pDNA [26]. Moreover, the presence of SC bands in the electrophoresis assay proved that nioplexe systems were able to protect the DNA from enzymatic degradation [9,10].

Once studied the physicochemical properties of P80PX niosomes we moved forward to the assessment of their transfection efficiency in primary cultures of hMSC monolayers. Our results showed that P80PX nioplexes prepared at 5/1 DOTMA/DNA ratio prompted the highest

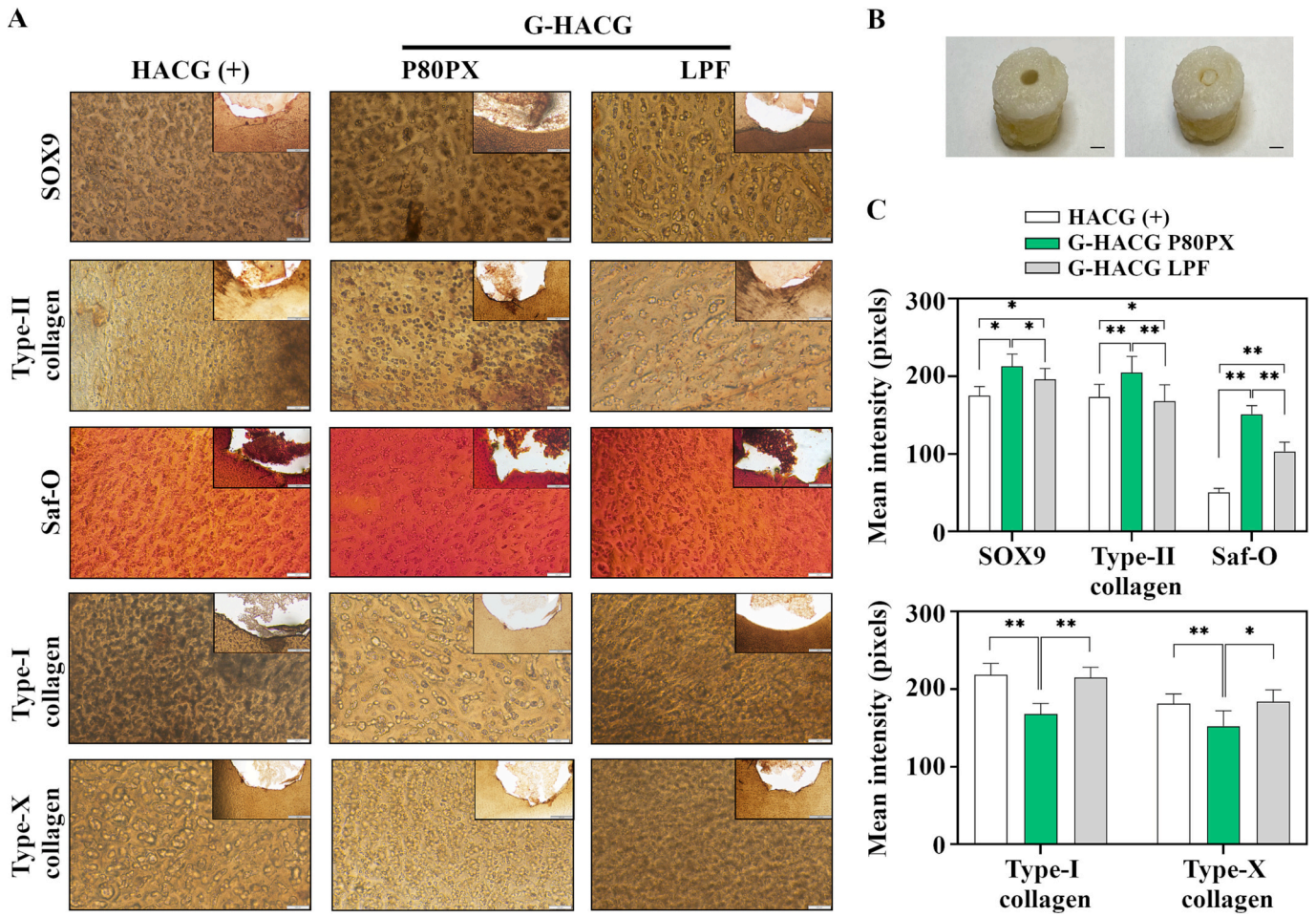

Fig. 8. Chondrogenesis of hMSCs seeded into HACGs, cultured in chondrogenic medium for 28 days (HACG (+), white), and transfected with p*sox9 via* P80PX (G-HACG P80PX, green) or LPF (G-HACG LPF, grey) in an *ex vivo* model of chondral defect. **(A)** Histological and immunohistochemical analyses for immunodetection of SOX9, type-I, type-II and type-X collagen, and Safranin-O, after 28 days of culture. All sections showed representative images of the focal defect adjacent area (scale bar 100 μm). Inserts showed top view of defects filled with different cryogel groups (scale bar 50 μm) (**B**) Representative macroscopic images of cartilage lesions empty (left) and filled with G-HACG P80PX (right) (scale bar 5 mm). (**C**) Histomorphometric analysis performed as described in Materials and Methods. *represent $p < 0.05$ and ** $p < 0.01$, when comparing denoted groups. (For interpretation of the references to colour in this figure legend, the reader is referred to the web version of this article.)

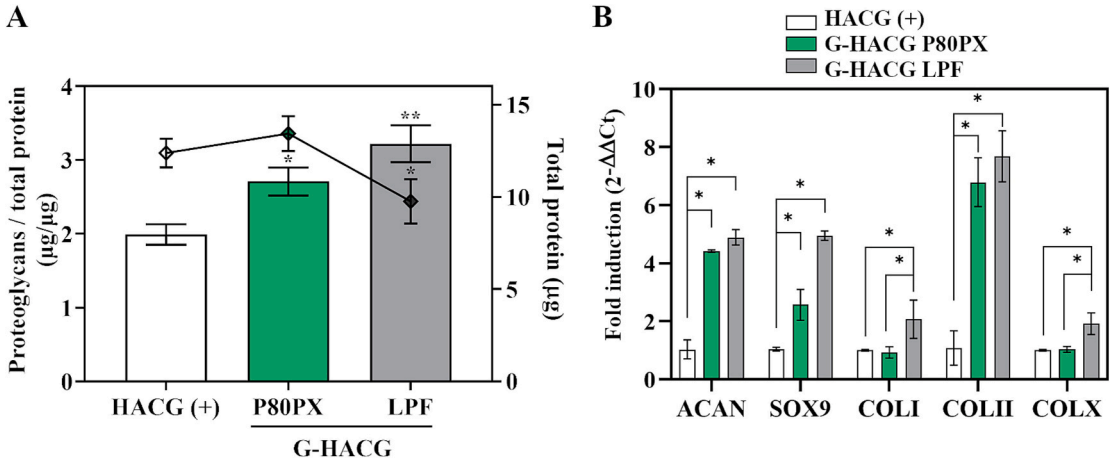

Fig. 9. Chondrogenesis of hMSCs seeded into HACGs, cultured in chondrogenic medium ((HACG (+), white), and transfected with p*sox9 via* P80PX (G-HACG P80PX, green) or LPF (G-HACG LPF, grey) in an *ex vivo* model of chondral defect. Samples were kept in culture for 28 days and processed for (**A**) proteoglycan contents standardized to the total protein contents and total protein contents and (**B**) Real time RT-PCR analysis of aggrecan (ACAN), the transcription factor SOX9, type-I collagen (COLI), type-II collagen (COLII), and type-X collagen (COLX) with RRN18s serving as a housekeeping gene and internal control (primers are listed in Section 2.6.3). Ct values were obtained for each target, and fold inductions were measured by using the $2^{-\Delta\Delta Ct}$ method. *represent $p < 0.05$ when comparing denoted groups. (For interpretation of the references to colour in this figure legend, the reader is referred to the web version of this article.)

transfection levels, without compromising cell viability. These results are in good agreement with previous observations using other niosome formulations, showing that a 5/1 ratio is enough to protect the DNA *cargo* mitigating the cytotoxic effects associated with higher doses of cationic lipid [9,26].

As endocytosis is the major route of cellular entry for non-viral vectors [27], we explored the internalization pathway of P80PX nioplexes in MSCs at 5/1 DOTMA/DNA ratio. A significant decrease in *lacZ* transgene expression was evident after cell pre-treatment with CHL and MβC, noticing a preferential internalization of P80PX nioplexes by clathrin-mediated endocytosis. This endocytic pathway has been reported to be the predominant route for internalization of lipoplex-like nanoparticles smaller than 500 nm [28], pointing out the relevance of an optimized endosomal escape mechanism to avoid lysosomal digestion.

The MSCs chondrogenesis is usually performed in 3D culture conditions to facilitate cell-cell and cell-extracellular matrix (ECM) interaction permitting cells to adapt their native morphology [10]. Cryogels were prepared by free-radical polymerization at −20°C of MetHA (5% *w/v*) producing highly macroporous matrices with a mean pore size of ~137 μm, being in the appropriate range (10–400 μm) to promote cell proliferation and homogeneous cell distribution [29]. Furthermore, the resulting cryogels exhibited percentages of swelling ratio and shape memory capacity of 95% and 98% respectively, being in the interval of those previously reported by others using alginate [30] or HA cryogels [13]. The rheology of the HACGs showed that the scaffolds were stable under stress conditions without leading to deformation. The storage modulus (G') decreases significantly from the dry to re-hydrated state of cryogels, noticing the soft spongy nature of the hydrated matrix. At body temperature (37°C) the viscoelastic behaviour of the cryogels remained constant, pointing out the suitability of the developed matrices for biomedical applications such as stem cell tissue engineering [11]. Finally, an evaluation of biodegradation capacity showed an appropriate time to replace damaged tissue with repaired tissue in cartilage engineering approaches, while limiting the existence of an immune response [13]. Previous studies have shown comparable degrees of degradation after 28 days (~30%) [31].

Incorporation of high concentrations of non-viral DNA complexes into hydrogel scaffolds has been shown to improve local gene delivery [21]. However physical encapsulation of these complexes often results in aggregation and inactivation problems that significantly precludes transfection efficiency. In order to solve these inconveniences, we incorporated sucrose into our P80PX formulations, based on previous studies confirming its potential as cryo and lyoprotector agent [20], and also on its ability to act as a lysosomotropic agent leading to an increase on MSCs transfection efficiency [9]. Effective incorporation of P80PX nioplexes inside the cryogels was verified by SEM. In good agreement with previous works using other GAMs [32] cumulative release profiles of HACGs showed a biphasic behaviour with an initial burst within the first day followed by a slower release up to 3 weeks. Moreover, freeze-drying of HACGs with P80PX nioplexes did not modify their release profile, retaining the pDNA released its bioactivity at all the conditions tested, and being increased during the initial time points [20].

Once incorporated P80PX nioplexes into HACG, we moved along MSCs seeding to obtain gene activated cryogels (G-HACG). Of note, *in situ* transfection of MSCs in G-HACG with P80PX nioplexes led to similar values of GFP expression to those achieved with the commercial reagent LPF, being in the range of those previously reported using similar niosome systems [21]. While the incorporation of a lysosomotropic agent into our formulation may be in part responsible for the increase in transfection achieved with P80PX nioplexes in 2D transfection studies [9], *in situ* transfection of MSCs in GAM has been proven to enhance both the transfection duration and transfection efficiency of non-viral vectors [6] Following the same tendency observed in 2D transfection assays, cell viability was higher in those G-HACG comprising P80PX complexes (G-HACG P80PX) when compared with LPF (G-HACG LPF) ones. Nonetheless, G-HACG P80PX exhibited a slight decrease in cell viability compared to the untransfected control group (HACG (+)). Such a reduction might be produced by GFP-induced apoptosis resulting from GFP aggregates or free radicals generation upon extended exposure time [33].

Chondrogenesis of MSCs under 3D conditions is generally preferred over traditional 2D cultures as more reliably mimics the natural conditions for cell proliferation and differentiation in cartilage tissue [6]. In this scenario, HA-based scaffolds have previously been shown to naturally promote MSCs differentiation due to the ubiquity of this biopolymer in the cartilage ECM [13]. Therefore, our next step was to test the capacity of G-HACGs to promote *in situ* chondrogenic differentiation of MSCs by substituting the reporter pGFP for a plasmid encoding the chondrogenic transcription factor SOX9. Effective transfection of MSCs in G-HACGs was evidenced by the intensity of SOX9 immunoreactivity and real-time RT-PCR analysis, showing an increase up to 2-fold compared to the untransfected controls (HACG (+)). Yet, in good concordance with previous studies [34], SOX9 overexpression led to a reduction in cell densities compared to untransfected control group (HACG (+). These observations agree with previous observations showing metabolic rather than proliferative effects of SOX9 [35]. Still and similarly to that observed in GFP *in situ* transfection, overexpression of this transcription factor *via* LPF lipoplexes (G-HACG LPF) led to a significantly descent on cell numbers compared with those matrices comprising P80PX nioplexes (G-HACG P80PX).

Overexpression of SOX9 led to an increase in hyaline cartilage markers as the deposition of type-II collagen and proteoglycans. These findings are in good agreement with previous studies using poly-ε-caprolactone scaffolds coated with recombinant adeno-associated viral vectors (rAAV) or RALA-pDNA complexes encoding for the transcription factor *sox9* to genetically modify MSCs [36] or bone marrow aspirates [14]. Further, also in good concordance with these studies [14,36] *in situ* transfection of MSCs allowed to limit undesirable osteogenic and hypertrophic differentiation events (matrix mineralization, type-I and type-X collagen expression) mostly in those cryogels containing P80PX nioplexes (G-HACGs P80PX) compared with those comprising LPF (G-HACGs LPF) [10]. This fact may be explained in part by the higher cytotoxicity observed in G-HACG LPF group that may entail their behaviour in favour to hypertrophic differentiation [37]. These results support the fact therapeutic gene delivery is highly dependent on the choice of the vector and does not directly correlate with therapeutic protein production [38].

Next, in order to establish the translatability of our system in a more natural and clinically relevant environment, we tested the ability of G-HACGs to promote cartilage reparative processes in an *ex vivo* model of cartilage defect generated in an osteochondral plug. This model has previously been shown to reproduce the natural joint environment more faithfully during culture compared to cartilage explants, maintaining the effects of soluble factors released by subchondral bone on chondrocytes [8]. Moreover, the *ex vivo* chondral defect model have demonstrated to be a very useful tool to explore OA mechanisms, drug screening and articular cartilage reparative strategies complying with the 3R (replace, reduce and refine) principles of animal experiments [8]. We also developed a vibroslice method for sectioning, avoiding dehydration and plastic or paraffin inclusion of the samples, maintaining the structural characteristic of the matrices assayed [24]. Consequently, the therapeutic potential of G-HACG was exclusively analysed on cartilage tissue adjacent to the lesions.

Overexpression of SOX9 in G-HACG led to a significant increase in the expression of this marker in the adjacent zones of the defects when compared with those ones filled with the untransfected HACG (+) control group. Most remarkably, overexpression of SOX9 in G-HACG significantly increased the expression of hyaline cartilage markers (type-II collagen and proteoglycans) in the cartilage regions adjacent to the defects when compared with those defects filled with HACG (+). These results are in good concordance with previous studies involving the

delivery of rAAV encoding for this transcription factor in a similar chondral defect model, supporting the idea on the effect of SOX9 in restoring cartilage extracellular matrix [39]. Lastly, also in good agreement with previous *ex vivo* [39] and *in vivo* [34,36,40] studies, a favourable decrease of hypertrophic events was noted in those defects filled with G-HACG, and mostly when comprising P80PX nioplexes (G-HACG P80PX).

Taken together the present study demonstrates the preliminary benefits of gene-activated cryogels *via* P80PX nioplexes in promoting cartilage reparative processes *in situ* and *ex vivo*. In spite of *in situ* transfection of MSCs into G-HACG P80PX constructs led to lower levels of SOX9 transgene expression than those achieved *via* G-HACG LPF matrices, it resulted in a marked lower cytotoxicity. Moreover, only G-HACG P80PX constructs promoted an effective chondrogenesis of MSCs by increasing the expression of hyaline-like cartilage markers, while avoiding the expression of undesired fibrocartilage and hypertrophic markers. From a clinical perspective this system may offer a potential "off the shelf" device to support improved cartilage repair by a minimally invasive administration. Still, further *in vivo* studies in relevant animal models of cartilage defects will be necessary to confirm the efficiency of these systems as a mean of developing new treatments for focal cartilage lesions.

Funding

The work was supported by MICINN [RTI2018-099389-A-100, RYC2018-025617-I], Xunta de Galicia [ED431F2021/10] and Deputación da Coruña [BINV-CS/2022, 2022000021445].

CRediT authorship contribution statement

Natalia Carballo-Pedrares: Data curation, Formal analysis, Methodology, Investigation, Writing - original draft, Writing - review & editing. **Junquera López-Seijas:** Formal analysis, Writing - review & editing. **Diego Miranda-Balbuena:** Investigation, Writing - review & editing. **Ibán Lamas:** Methodology, Resources. **Julián Yáñez:** Methodology, Resources, Writing - review & editing. **Ana Rey-Rico:** Data curation, Formal analysis, Funding acquisition, Investigation, Methodology, Conceptualization, Project administration, Resources, Supervision, Writing - original draft, Writing - review & editing.

Data availability

Data will be made available on request.

Acknowledgements

We would like to acknowledge Prof. M. Cucchiarini for providing pACP-h*sox9* (p*sox9*, bp 6,915). We also thank Biobanco de A Coruña from SERGAS for providing biological samples, BASF (Ludwigshafen, Germany) for supplying the poloxamer 407 and Universidade da Coruña/CISUG for the funding for open access charge.

Appendix A. Supplementary data

Supplementary data to this article can be found online at https://doi.org/10.1016/j.jconrel.2023.09.008.

References

[1] J.M. Hootman, C.G. Helmick, Projections of US prevalence of arthritis and associated activity limitations, Arthritis Rheumatol. 54 (2006) 226–229, https://doi.org/10.1002/ART.21562.
[2] M. Cucchiarini, A. Rey-Rico, Controlled gene delivery systems for articular cartilage repair, in: Adv. Biomater. Biomed. Appl., Springer, 2017, pp. 261–300, https://doi.org/10.1007/978-981-10-3328-5_7.
[3] H. Madry, J.K. Venkatesan, N. Carballo-pedrares, A. Rey-rico, M. Cucchiarini, Scaffold-mediated gene delivery for osteochondral repair, Pharmaceutics 12 (2020) 1–23, https://doi.org/10.3390/PHARMACEUTICS12100930.
[4] H. Zu, D. Gao, Non-viral vectors in gene therapy: recent development, challenges, and prospects, AAPS J. 23 (2021) 78, https://doi.org/10.1208/S12248-021-00608-7.
[5] J. Fang, Y.Y. Zhu, E. Smiley, J. Bonadio, J.P. Rouleau, S.A. Goldstein, L. K. Mccauley, B.L. Davidson, B.J. Roessler, Stimulation of new bone formation by direct transfer of osteogenic plasmid genes, Proc. Natl. Acad. Sci. U. S. A. 93 (1996) 5753, https://doi.org/10.1073/PNAS.93.12.5753.
[6] S. Raisin, E. Belamie, M. Morille, Non-viral gene activated matrices for mesenchymal stem cells based tissue engineering of bone and cartilage, Biomaterials 104 (2016) 223–237, https://doi.org/10.1016/J.BIOMATERIALS.2016.07.017.
[7] C.J. Needham, S.R. Shah, R.L. Dahlin, L.A. Kinard, J. Lam, B.M. Watson, S. Lu, F. K. Kasper, A.G. Mikos, Osteochondral tissue regeneration through polymeric delivery of DNA encoding for the SOX trio and RUNX2, Acta Biomater. 10 (2014) 4103–4112, https://doi.org/10.1016/J.ACTBIO.2014.05.011.
[8] K.H. Li, Y. Zhu, P.H. Zhang, M. Alini, S. Grad, Z. Li, Osteochondral explants for diarthrodial joint diseases: bridging the gap between bench and bedside, Eur. Cell. Mater. 44 (2022) 74–89, https://doi.org/10.22203/ECM.V044A05.
[9] N. Carballo-Pedrares, A. Kattar, A. Concheiro, C. Alvarez-Lorenzo, A. Rey-Rico, Niosomes-based gene delivery systems for effective transfection of human mesenchymal stem cells, Mater. Sci. Eng. C 128 (2021) 112307, https://doi.org/10.1016/J.MSEC.2021.112307.
[10] N. Carballo-Pedrares, C. Sanjurjo-Rodriguez, J. Señarís, S. Díaz-Prado, A. Rey-Rico, Chondrogenic differentiation of human mesenchymal stem cells via SOX9 delivery in cationic niosomes, Pharmaceutics 14 (2022) 2327, https://doi.org/10.3390/PHARMACEUTICS14112327/S1.
[11] M. Razavi, Y. Qiao, A.S. Thakor, Three-dimensional cryogels for biomedical applications, J. Biomed. Mater. Res. - Part A. 107 (2019) 2736–2755, https://doi.org/10.1002/jbm.a.36777.
[12] L. Cheng, K. Ji, T.Y. Shih, A. Haddad, G. Giatsidis, D.J. Mooney, D.P. Orgill, C. S. Nabzdyk, Injectable shape-memorizing three-dimensional hyaluronic acid cryogels for skin sculpting and soft tissue reconstruction, Tissue Eng. - Part A 23 (2017) 243–251, https://doi.org/10.1089/TEN.TEA.2016.0263.
[13] T. He, B. Li, T. Colombani, K. Joshi-Navare, S. Mehta, J. Kisiday, S.A. Bencherif, A. G. Bajpayee, Hyaluronic acid-based shape-memory cryogel scaffolds for focal cartilage defect repair, Tissue Eng. - Part A 27 (2021) 748–760, https://doi.org/10.1089/TEN.TEA.2020.0264.
[14] J.K. Venkatesan, W. Meng, A. Rey-Rico, G. Schmitt, S. Speicher-Mentges, C. Falentin-Daudré, A. Leroux, H. Madry, V. Migonney, M. Cucchiarini, Enhanced chondrogenic differentiation activities in human bone marrow aspirates via sox9 overexpression mediated by pNaSS-grafted PCL film-guided rAAV gene transfer, Pharmaceutics 12 (2020) 280, https://doi.org/10.3390/PHARMACEUTICS12030280.
[15] E. Ojeda, M. Agirre, I. Villate-Beitia, M. Mashal, G. Puras, J. Zarate, J.L. Pedraz, Elaboration and physicochemical characterization of niosome-based nioplexes for gene delivery purposes, Methods Mol. Biol. 1445 (2016) 63–75, https://doi.org/10.1007/978-1-4939-3718-9_5.
[16] L.D.F. Almeida, P.S. Babo, C.R. Silva, M.T. Rodrigues, J. Hebling, R.L. Reis, M. E. Gomes, Hyaluronic acid hydrogels incorporating platelet lysate enhance human pulp cell proliferation and differentiation, J. Mater. Sci. 29 (2018) 88, https://doi.org/10.1007/S10856-018-6088-7.
[17] E. Tsanaktsidou, O. Kammona, C. Kiparissides, On the synthesis and characterization of biofunctional hyaluronic acid based injectable hydrogels for the repair of cartilage lesions, Eur. Polym. J. 114 (2019) 47–56, https://doi.org/10.1016/j.eurpolymj.2019.02.024.
[18] F. Jonidi Shariatzadeh, A. Solouk, S. Bagheri Khoulenjani, S. Bonakdar, H. Mirzadeh, Injectable and reversible preformed cryogels based on chemically crosslinked gelatin methacrylate (GelMA) and physically crosslinked hyaluronic acid (HA) for soft tissue engineering, Colloids Surf. B Biointerfaces 203 (2021) 111725, https://doi.org/10.1016/J.COLSURFB.2021.111725.
[19] C. Calitz, N. Pavlovic, J. Rosenquist, C. Zagami, S. Ayan, F. Heindryckx, A biomimetic model for liver cancer to study tumor-stroma interactions in a 3D environment with tunable bio-physical properties, J. Vis. Exp. 7 (2020) 162, https://doi.org/10.3791/61606.
[20] Y. Lei, S. Huang, P. Sharif-Kashani, Y. Chen, P. Kavehpour, T. Segura, Incorporation of active DNA/cationic polymer polyplexes into hydrogel scaffolds, Biomaterials 31 (2010) 9106–9116, https://doi.org/10.1016/J.BIOMATERIALS.2010.08.016.
[21] I. Villate-Beitia, N.F. Truong, I. Gallego, J. Zárate, G. Puras, J.L. Pedraz, T. Segura, Hyaluronic acid hydrogel scaffolds loaded with cationic niosomes for efficient non-viral gene delivery, RSC Adv. 8 (2018) 31934–31942, https://doi.org/10.1039/C8RA05125A.
[22] C.T. Huynh, M.K. Nguyen, G.Y. Tonga, L. Longé, V.M. Rotello, E. Alsberg, Photocleavable hydrogels for light-triggered siRNA release, Adv. Healthc. Mater. 5 (2016) 305–310, https://doi.org/10.1002/ADHM.201500778.
[23] S. Duchi, S. Doyle, T. Eekel, C.D. O'Connell, C. Augustine, P. Choong, C. Onofrillo, C. Di Bella, Protocols for culturing and imaging a human ex vivo osteochondral model for cartilage biomanufacturing applications, Materials (Basel, Switzerland) 12 (2019) 640, https://doi.org/10.3390/MA12040640.
[24] A.R. Short, C. Czeisler, B. Stocker, S. Cole, J.J. Otero, J.O. Winter, Imaging cell–matrix interactions in 3D collagen hydrogel culture systems, Macromol. Biosci. 17 (2017) 1600478, https://doi.org/10.1002/MABI.201600478.

[25] S. Grijalvo, G. Puras, J. Zárate, M. Sainz-Ramos, N.A.L.L. Qtaish, T. López, M. Mashal, N. Attia, D. Díaz, R. Pons, E. Fernández, J.L. Pedraz, R. Eritja, Cationic niosomes as non-viral vehicles for nucleic acids: challenges and opportunities in gene delivery, Pharmaceutics 11 (2019) 50, https://doi.org/10.3390/PHARMACEUTICS11020050.

[26] M. Sainz-Ramos, I. Villate-Beitia, I. Gallego, N.A.L. Qtaish, M. Menéndez, L. Lagartera, S. Grijalvo, R. Eritja, G. Puras, J.L. Pedraz, Correlation between biophysical properties of niosomes elaborated with chloroquine and different tensioactives and their transfection efficiency, Pharmaceutics 13 (2021) 1787, https://doi.org/10.3390/PHARMACEUTICS13111787.

[27] W. Liang, J.K.W. Lam, Endosomal escape pathways for non-viral nucleic acid delivery systems, in: Mol. Regul. Endocytosis, InTech, 2012, pp. 429–456, https://doi.org/10.5772/46006.

[28] J. Rejman, M. Conese, D. Hoekstra, Gene transfer by means of lipo- and polyplexes: role of clathrin and caveolae-mediated endocytosis, J. Liposome Res. 16 (2006) 237–247, https://doi.org/10.1080/08982100600848819.

[29] L.J. Eggermont, Z.J. Rogers, T. Colombani, A. Memic, S.A. Bencherif, Injectable cryogels for biomedical applications, Trends Biotechnol. 38 (2020) 418–431, https://doi.org/10.1016/J.TIBTECH.2019.09.008.

[30] S.A. Bencherif, R.W. Sands, D. Bhatta, P. Arany, C.S. Verbeke, D.A. Edwards, D. J. Mooney, Injectable preformed scaffolds with shape-memory properties, Proc. Natl. Acad. Sci. U. S. A. 109 (2012) 19590–19595, https://doi.org/10.1073/PNAS.1211516109.

[31] M. Wang, J. Hu, Y. Ou, X. He, Y. Wang, C. Zou, Y. Jiang, F. Luo, D. Lu, Z. Li, J. Li, H. Tan, Shape-recoverable hyaluronic acid-waterborne polyurethane hybrid cryogel accelerates hemostasis and wound healing, ACS Appl. Mater. Interfaces 14 (2022) 17093–17108, https://doi.org/10.1021/ACSAMI.2C01310.

[32] S. Gojgini, T. Tokatlian, T. Segura, Utilizing cell-matrix interactions to modulate gene transfer to stem cells inside hyaluronic acid hydrogels, Mol. Pharm. 8 (2011) 1582–1591, https://doi.org/10.1021/MP200171D.

[33] E.C. Jensen, Use of fluorescent probes: their effect on cell biology and limitations, Anat. Rec. 295 (2012) 2031–2036, https://doi.org/10.1002/AR.22602.

[34] C. Lange, H. Madry, J.K. Venkatesan, G. Schmitt, S. Speicher-Mentges, D. Zurakowski, M.D. Menger, M.W. Laschke, M. Cucchiarini, rAAV-mediated sox9 overexpression improves the repair of osteochondral defects in a clinically relevant large animal model over time in vivo and reduces perifocal osteoarthritic changes, Am. J. Sports Med. 49 (2021) 3696–3707, https://doi.org/10.1177/03635465211049414.

[35] L. Kupcsik, M.J. Stoddart, Z. Li, L.M. Benneker, M. Alini, Improving chondrogenesis: potential and limitations of SOX9 gene transfer and mechanical stimulation for cartilage tissue engineering, Tissue Eng. - Part A 16 (2010) 1845–1855, https://doi.org/10.1089/TEN.TEA.2009.0531.

[36] T. Gonzalez-Fernandez, S. Rathan, C. Hobbs, P. Pitacco, F.E. Freeman, G. M. Cunniffe, N.J. Dunne, H.O. McCarthy, V. Nicolosi, F.J. O'Brien, D.J. Kelly, Pore-forming bioinks to enable spatio-temporally defined gene delivery in bioprinted tissues, J. Control. Release 301 (2019) 13–27, https://doi.org/10.1016/J.JCONREL.2019.03.006.

[37] S. Chameettachal, S. Midha, S. Ghosh, Regulation of chondrogenesis and hypertrophy in silk fibroin-gelatin-based 3D bioprinted constructs, ACS Biomater Sci. Eng. 2 (2016) 1450–1463, https://doi.org/10.1021/ACSBIOMATERIALS.6B00152.

[38] T. Gonzalez-Fernandez, B.N. Sathy, C. Hobbs, G.M. Cunniffe, H.O. McCarthy, N. J. Dunne, V. Nicolosi, F.J. O'Brien, D.J. Kelly, Mesenchymal stem cell fate following non-viral gene transfection strongly depends on the choice of delivery vector, Acta Biomater. 55 (2017) 226–238, https://doi.org/10.1016/J.ACTBIO.2017.03.044.

[39] A. Rey-Rico, J.K. Venkatesan, G. Schmitt, S. Speicher-Mentges, H. Madry, M. Cucchiarini, Effective remodelling of human osteoarthritic cartilage by sox9 gene transfer and overexpression upon delivery of rAAV vectors in polymeric micelles, Mol. Pharm. 15 (2018) 2816–2826, https://doi.org/10.1021/ACS.MOLPHARMACEUT.8B00331.

[40] M. Cucchiarini, P. Orth, H. Madry, Direct rAAV SOX9 administration for durable articular cartilage repair with delayed terminal differentiation and hypertrophy in vivo, J. Mol. Med. 91 (2013) 625–636, https://doi.org/10.1007/S00109-012-0978-9.